Eur. Phys. J. C 29, 521–530 (2003)
Digital Object Identifier (DOI) 10.1140/epjc/s2003-01236-y

THE EUROPEAN PHYSICAL JOURNAL C

Screening effects in the ultra-high energy neutrino interactions

K. Kutak, J. Kwieciński

H. Niewodniczański Institute of Nuclear Physics, Kraków, Poland

Received: 26 March 2003 / Revised version: 17 April 2003 /
Published online: 3 July 2003 – © Springer-Verlag / Società Italiana di Fisica 2003

Abstract. We study possible saturation effects in the total cross-sections describing the interaction of ultra-high energy neutrinos with nucleons. This analysis is performed within two approaches, i.e., within the Golec-Biernat–Wüsthoff saturation model and within the scheme unifying the DGLAP and BFKL dynamics incorporating non-linear screening effects which follow from the Balitzki–Kovchegov equation. The structure functions in both approaches are constrained by HERA data. It is found that screening effects affect the extrapolation of the neutrino–nucleon total cross-sections to ultra-high neutrino energies E_ν and reduce their magnitude by a factor equal to about 2 at $E_\nu \sim 10^{12}\,\mathrm{GeV}$. This reduction becomes amplified by nuclear shadowing in the case of the neutrino–nucleus cross-sections and an approximate estimate of this effect is performed.

1 Introduction

Ultra-high energy neutrinos are one of the components of the spectrum of particles that reach Earth. As they interact weakly with matter their propagation through interstellar space is not attenuated. This is the reason why they are unique carriers of information about distant objects such as GRB (gamma ray bursts), AGN (active gallactic nuclei) etc. which are most probably their sources. This information can be studied by neutrino telescopes [1].

Attenuation of neutrinos traversing the Earth and their detection depend upon the cross-sections describing the interaction of neutrinos with nucleons and atomic nuclei. Ultra-high energy neutrino interactions with nucleons are sensitive to the behavior of the nucleon structure functions at extremely small values of the Bjorken parameter x and relatively large scales $Q^2 \sim M_W^2$ [2–5]. Here, as usual $x = Q^2/(2pq)$, where $Q^2 = -q^2$ with p and q denoting the four-momentum of the nucleon and four-momentum transfer between the leptons in the inelastic neutrino–nucleon interaction respectively. The values of x which can be probed can be several orders of magnitude smaller than those which are currently accessible at HERA [6] and, for instance for neutrino energies $E_\nu \sim 10^{12}\,\mathrm{GeV}$, typical values of x which contribute to the neutrino cross-sections can be as small as $x \sim 10^{-8}$. A reliable estimate of the ultra-high energy neutrino cross-sections does therefore require a reliable extrapolation of the structure functions towards the region of very small values of x and large Q^2, i.e. far beyond the region which is currently accessible. Existing estimates of the neutrino cross-sections with structure functions constrained by HERA data are based on either a DGLAP [2,4,5] or an extended BFKL [3] *linear* evolution which neglects non-linear screening effects [7–14]. Those effects are in general expected to slow down the increase of the parton distributions and of the cross-sections with decreasing x and to reduce their magnitude. Possible implications of screening effects for the estimate of the ultra-high energy cross-sections have recently been discussed in [15–18] with somewhat conflicting conclusions. Thus in [15,16] it has been claimed that the screening effects should play a negligible role in the estimate of the ultra-high energy neutrino cross-sections due to the dominance of the relatively large scales $Q^2 \sim M_W^2$. On the contrary, results obtained in [18] seem to imply that they may be significant and, moreover, when combined with the BFKL dynamics may even lead to enhancement of the cross-sections.

The purpose of this paper is to present a relatively detailed and realistic estimate of the impact of the screening effects on the cross-sections describing ultra-high energy neutrino interactions. We perform this analysis within the two frameworks which incorporate screening effects, i.e. the Golec-Biernat–Wüsthoff (GBW) model [19] and the unified BFKL/DGLAP scheme [3,20] supplemented by the non-linear term in the corresponding evolution equations. This term will be obtained from the non-linear part of the Balitzki–Kovchegov (BK) equation [12,13]. In both cases the parton distributions and the resulting cross-sections will be constrained by the HERA data. The content of our paper is as follows. In the next section we recollect basic formulas describing the deep inelastic neutrino–nucleon scattering. In Sect. 3 we discuss the description of deep inelastic scattering within the dipole picture and present results for neutrino cross-sections calculated within the GBW model. Section 4 contains a formulation of the unified BFKL/DGLAP evolution equations supplemented by non-linear screening effects and results for neutrino cross-sections calculated within this approach. Section 5 contains a summary and our conclusions.

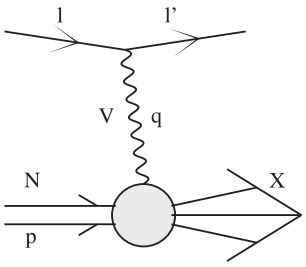

Fig. 1. Deep inelastic scattering

2 Basic formulas describing the deep inelastic neutrino scattering

Deep inelastic neutrino scattering is illustrated by the diagram in Fig. 1. It can proceed through $W^{\pm}$ or Z^0 exchanges, which corresponds to charged current (CC) or neutral current (NC) interactions respectively. The charged current interactions correspond to the processes $\nu + N \to l^- + X$ ($\bar{\nu} + N \to l^+ + X$) with charged leptons $l^{\pm}$ in the final state, while the neutral current interactions correspond to the processes $\nu + N \to \nu + X$ ($\bar{\nu} + N \to \bar{\nu} + X$). The standard kinematical variables describing these processes are

$$\begin{aligned} s &= 2ME, \\ Q^2 &= -q^2, \\ x &= \frac{Q^2}{2pq}, \\ y &= \frac{pq}{ME}, \end{aligned} \tag{1}$$

where M is the nucleon mass, E denotes the neutrino energy, while p and q are the four momenta of the nucleon and of the exchanged boson respectively. The cross-sections describing deep inelastic neutrino scattering are expressed in the following way in terms of the structure functions $F_2^{\mathrm{CC,NC}}(x,Q^2)$, $F_{\mathrm{L}}^{\mathrm{CC,NC}}(x,Q^2)$ and $F_3^{\mathrm{CC,NC}}(x,Q^2)$:

$$\begin{aligned} &\frac{\partial^2\sigma_{\nu,\bar{\nu}}^{\mathrm{CC,NC}}}{\partial x\partial y} = \frac{G_{\mathrm{F}}^2 ME}{\pi}\left(\frac{M_i^2}{Q^2+M_i^2}\right)^2 \\ &\times\left[\frac{1+(1-y)^2}{2}F_2^{\mathrm{CC,NC}}(x,Q^2) - \frac{y^2}{2}F_{\mathrm{L}}^{\mathrm{CC,NC}}(x,Q^2)\right. \\ &\left.\pm\, y\left(1-\frac{y}{2}\right)xF_3^{\mathrm{CC,NC}}(x,Q^2)\right], \end{aligned} \tag{2}$$

where G_{F} is the Fermi constant and M_i denotes the mass of the charged ($W^{\pm}$) or neutral (Z^0) gauge boson.

In the QCD improved parton model the structure functions $F_{2,3}(x,Q^2)$ are expressed in terms of the (scale dependent) quark and antiquark distributions [23]. Thus for the isoscalar target $N = \frac{n+p}{2}$ we have

$$\begin{aligned} F_2^{\mathrm{CC}}(x,Q^2) &= x[u_v(x,Q^2)+d_v(x,Q^2)] \\ &+ 2x[\bar{u}(x,Q^2)+\bar{d}(x,Q^2)+s(x,Q^2)+c(x,Q^2)], \end{aligned} \tag{3}$$

$$F_3^{\mathrm{CC}}(x,Q^2) = u_v(x,Q^2)+d_v(x,Q^2), \tag{4}$$

$$\begin{aligned} F_2^{\mathrm{NC}}(x,Q^2) &= \frac{(L_u^2+L_d^2+R_u^2+R_d^2)}{4} \\ &\times\{[u_v(x,Q^2)+d_v(x,Q^2)] \\ &+2x[\bar{u}(x,Q^2)+\bar{d}(x,Q^2)+s(x,Q^2)+c(x,Q^2)]\}, \end{aligned} \tag{5}$$

$$\begin{aligned} &F_3^{\mathrm{CC}}(x,Q^2) \\ &= \frac{(L_u^2+L_d^2-R_u^2-R_d^2)}{4}[u_v(x,Q^2)+d_v], \end{aligned} \tag{6}$$

where the chiral couplings can be expressed in terms of the Weinberg angle θ_{W}

$$\begin{aligned} L_u &= 1-\frac{4}{3}\sin^2\theta_{\mathrm{W}}, \\ L_d &= -1+\frac{2}{3}\sin^2\theta_{\mathrm{W}}, \\ R_u &= -\frac{4}{3}\sin^2\theta_{\mathrm{W}}, \\ R_d &= \frac{2}{3}\sin^2\theta_{\mathrm{W}}. \end{aligned} \tag{7}$$

The quantities which are relevant for the quantitative description of the penetration of ultra-high energy neutrinos through Earth and for their detection are the neutrino cross-sections integrated over available phase space at the given neutrino energy. These integrated cross-section are given by

$$\sigma_{\nu,\bar{\nu}}^{\mathrm{CC,NC}}(E) = \int_{Q^2_{\min}}^{s} \mathrm{d}Q^2 \int_{Q^2/s}^{1} \mathrm{d}x \frac{1}{xs}\frac{\partial^2\sigma_{\nu,\bar{\nu}}^{\mathrm{CC,NC}}}{\partial x\partial y}, \tag{8}$$

with $y = Q^2/(xs)$. In (8) we have introduced the minimal value $Q^2_{\min}$ of Q^2 in order to stay in the deep inelastic region. In our calculations we set $Q^2_{\min} = 1\,\mathrm{GeV}^2$. In the "low" energy region $s < M_i^2$ the integrated cross-sections increases linearly with E and in this region the interaction with valence quarks dominates. In the high energy region the contribution of valence quarks saturates and the energy dependence of $\sigma_{\nu,\bar{\nu}}^{\mathrm{CC,NC}}(E)$ is driven by the small x behavior of the sea quark distributions [3]. It is this part of the cross-sections which will be analyzed in our paper.

Existing numerical estimates of the ultra-high energy cross-sections are based upon extrapolation of the parton distributions towards the very small x region using linear (DGLAP and/or BFKL) QCD evolution equations [2–4]. At small x the dominant partons are the gluons, and the sea quark distributions are driven by the gluons through the $g \to q\bar{q}$ transitions. The linear QCD evolution generates an indefinite increase of gluon distributions with decreasing x, which implies a similar increase of the sea quark distributions and of the structure functions $F_2^{\mathrm{CC,NC}}(x,Q^2)$ and $F_{\mathrm{L}}^{\mathrm{CC,NC}}(x,Q^2)$. This increase is tamed by the non-linear screening effects which lead to saturation [7–13]. An efficient way of introducing saturation can be realized using the color dipole framework in which the DIS

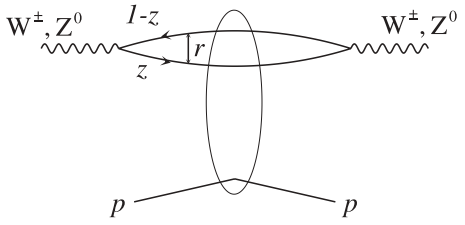

Fig. 2. Schematic representation of the dipole picture [19]

at low x is viewed as the result of the interaction of the color $q\bar{q}$ dipole which the gauge bosons fluctuate to as illustrated in Fig. 2. A very succesful semi-phenomenolgical analysis of ep DIS at low x has been performed within this framework by Golec-Biernat and Wüsthoff [19] and in the next section we apply this model to the estimate of the saturation effects in the ultra-high energy neutrino cross-sections.

3 DIS in the dipole picture and ultra-high energy neutrino interactions

The DIS structure functions in the dipole picture can be written in the following form [19]:

$$F_{\mathrm{T,L}}^{\mathrm{CC,NC}}(x,Q^2) = \frac{Q^2}{4\pi^2}\int \mathrm{d}^2\mathbf{r}\int_0^1 \mathrm{d}z|\bar{\psi}_{\mathrm{T,L}}^{W,Z}(r,z,Q^2)|^2\sigma_d(r,x). \quad (9)$$

In this equation r denotes the transverse size of the $q\bar{q}$ dipole, z the longitudinal momentum fraction carried by a quark and the $\bar{\psi}_{\mathrm{T,L}}^{W,Z}(r,z,Q^2)$ are proportional to the wave functions of the (virtual) charged or neutral gauge bosons corresponding to their transverse or longitudinal polarization ($F_{\mathrm{T}}^{\mathrm{CC,NC}}(x,Q^2) = F_2^{\mathrm{CC,NC}}(x,Q^2) - F_{\mathrm{L}}^{\mathrm{CC,NC}}(x,Q^2)$). Explicit expressions for $\bar{\psi}_{\mathrm{T,L}}^{W,Z}(r,z,Q^2)$ are given below. The cross-section $\sigma_d(r,x)$ describes the interaction of the color $q\bar{q}$ dipole with the nucleon. In the GBW model $\sigma_d(r,x)$ has the following form:

$$\sigma_d(r,x) = \sigma_0\left[1-\exp\left(-\frac{r^2}{4R_0^2(x)}\right)\right]. \quad (10)$$

The most crucial element in this model is the adoption of the x-dependent saturation radius $R_0(x)$ which scales the $q\bar{q}$ separation in the dipole cross-section. The saturation radius is a decreasing function with decreasing x and is parameterized as below:

$$R_0^2(x) = \frac{1}{Q_0^2}\left(\frac{x}{x_0}\right)^{\lambda}, \quad (11)$$

with $Q_0^2 = 1\,\mathrm{GeV}^2$. The three parameters of the model σ_0, λ and x_0 were fitted to inclusive DIS data from HERA for $x < 0.01$. We shall use the following values: $\sigma_0 = 29.12\,\mathrm{mb}$, $\lambda = 0.2777$ and $x_0 = 0.41\times10^{-4}$, which were obtained from the fit with four flavors.

In the limit $r \to \infty$ we have $\sigma_d \to \sigma_0$, i.e. the dipole cross-section exhibits the saturation property. The fact that the dipole cross-section is limited by the energy independent cross-section can be regarded as the unitarity bound. In the limit $r \to 0$ the dipole cross-section vanishes, reflecting the color transparency.

The GBW model, which has proved to be phenomenologically very succesful in describing HERA data and has embodied saturation can be used for the estimate of the UHE neutrino cross-sections. In our calculation of the UHE neutrino–nucleon cross-section we consider only four flavors (u,d,s,c). The corresponding $q\bar{q}$ dipoles which contribute to Cabibbo favored transitions are $u\bar{d}$ $(d\bar{u})$, $c\bar{s}$ $(s\bar{c})$ for charged currents and $u\bar{u}, d\bar{d}, c\bar{c}, s\bar{s}$ for neutral currents respectively. In our calculations we shall assume massless quarks. This approximation is reasonable for very high energy neutrinos. A possible contribution of the heavy quarks (b,t), where the mass parameters cannot be neglected, is found to be relatively small [3].

The dipole model describes well deep inelastic scattering at small x, but it becomes inaccurate at large and moderately small values of x. This is closely linked with the fact that it neglects theoretical expectations concerning the behavior of the quark distributions in the $x \to 1$ limit. This effect can be approximately taken into account by multiplying the structure functions by a factor $(1-x)^{2n_s-1}$ which follows from the constitutent counting rule where n_s denotes the number of spectator quarks. Since the dipole model represents the sea quark contribution we set $n_s = 4$.

The functions $\bar{\psi}_{\mathrm{T,L}}^{W,Z}(r,z,Q^2)$ corresponding to the sum over dipoles corresponding to massless quarks are given by the following formulas:

$$|\bar{\psi}_{\mathrm{T}}^{W}(r,z,Q^2)|^2 = \frac{6}{\pi^2}[z^2+(1-z)^2]\bar{Q}^2K_1^2(\bar{Q}r), \quad (12)$$

$$|\bar{\psi}_{\mathrm{L}}^{W}(r,z,Q^2)|^2 = \frac{24}{\pi^2}z^2(1-z)^2Q^2K_0^2(\bar{Q}r), \quad (13)$$

$$|\bar{\psi}_{\mathrm{T}}^{Z}(r,z,Q^2)|^2 = \frac{3}{2\pi^2}(L_u^2+L_d^2+R_u^2+R_d^2)[z^2+(1-z)^2]\bar{Q}^2K_1^2(\bar{Q}r), \quad (14)$$

$$|\bar{\psi}_{\mathrm{L}}^{Z}(r,z,Q^2)|^2 = \frac{6}{\pi^2}(L_u^2+L_d^2+R_u^2+R_d^2)z^2(1-z)^2Q^2K_0^2(\bar{Q}r), \quad (15)$$

where

$$\bar{Q}^2 = z(1-z)Q^2, \quad (16)$$

and $K_{0,1}(u)$ are the McDonald's functions.

In Figs. 3 and 4 we show results for the ultra-high neutrino cross-sections calculated within the GBW saturation model and confront them with the estimate based upon the unified BFKL/DGLAP framework which ignored saturation effects [3]. We can see that the cross-sections calculated within the GBW model are at ultra-high energies, $E \sim 10^{12}\,\mathrm{GeV}$, about a factor two smaller than those which were estimated within the scheme incorporating BFKL and DGLAP evolution without screening corrections.

It should however be remembered that the GBW model has been tested phenomenologically for relatively

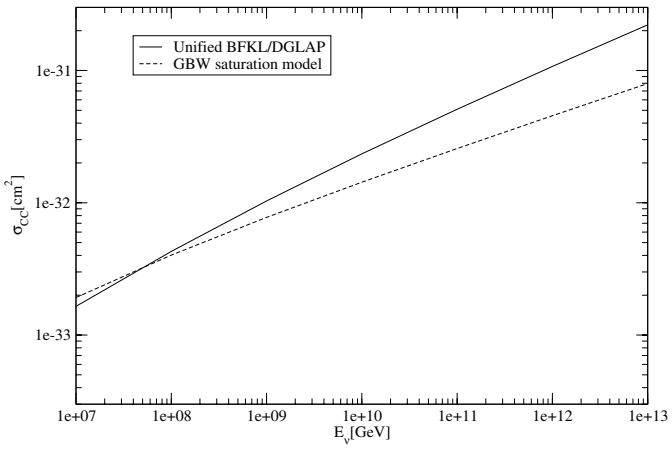

Fig. 3. The prediction for the neutrino–nucleon CC cross-section obtained from the GBW saturation model. For comparison we also show results based on the (linear) unified BFKL/DGLAP evolution

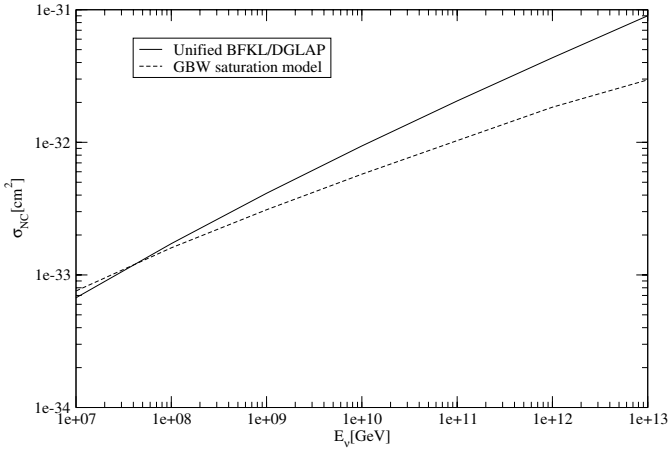

Fig. 4. As for Fig. 2, but for the NC interactions

low values of Q^2 and that it requires corrections incorporating DGLAP evolution [21]. It is therefore necessary to perform an estimate of the neutrino cross-sections within the scheme that would include saturation effects together with complete QCD evolution as will be described in the next section.

4 Unified BFKL/DGLAP evolution with non-linear screening effects and ultra-high neutrino cross-sections

We have shown in the previous section that the ultra-high energy neutrino cross-sections based upon the GBW saturation model are at very high neutrino energies ($E > 10^{12}$ GeV) about a factor two smaller than those calculated from the linear QCD evolution equations. It can however be expected that part of this reduction may just be caused by the fact that the GBW model does not correctly include the QCD evolution effects [21]. Let us recall that the dominant contribution to the neutrino cross-sections comes from the region $Q^2 \sim M_W^2$, where the simple GBW model may not be sufficiently accurate. It would therefore be desirable to discuss the ultra-high energy cross-sections within the framework which contains both the QCD evolution effects and saturation. It is also of course very important that this framework should be based upon realistic parton distributions constrained by HERA data. The framework should also contain all the QCD expectations concerning the small x behavior which follow from the BFKL dynamics as discussed, for instance, in [20]. We shall therefore use the scheme developed in [20] containing the unified BFKL/DGLAP dynamics with subleading BFKL effects taken into account and supplement it by the screening contributions for the gluon distributions. To be precise we shall include the non-linear screening term in the corresponding equation for the unintegrated gluon distribution $f(x,k^2)$, where k^2 is the transverse momentum squared of the gluon [20]. The structure functions are then calculated from the unintegrated gluon distributions using the k_t factorization prescription [25]. The extended system of the evolution equations with screening effects included then reads

$$
\begin{aligned}
f(x,k^2) &= \tilde{f}^{(0)}\left(x,k^2\right) \\
&+ 2N_c \frac{\alpha_{\mathrm{s}}\left(k^2\right)}{2\pi} k^2 \int_x^1 \frac{\mathrm{d}z}{z} \int_{k_0^2} \frac{\mathrm{d}k'^2}{k'^2} \\
&\quad \times \left\{ \frac{f\left(\frac{x}{z},k'^2\right)\Theta\left(\frac{k^2}{z}-k'^2\right) - f\left(\frac{x}{z},k^2\right)}{|k'^2-k^2|} \right. \\
&\quad \left. + \frac{f\left(\frac{x}{z},k^2\right)}{\left[4k'^4+k^4\right]^{\frac{1}{2}}} \right\} \\
&+ \frac{\alpha_{\mathrm{s}}\left(k^2\right)}{2\pi} \int_x^1 \frac{\mathrm{d}z}{z} \\
&\quad \times \left[\left(zP_{gg}(z) - 2N_c\right) \int_{k_0^2}^{k^2} \frac{\mathrm{d}k'^2}{k'^2} f\left(\frac{x}{z},k'^2\right) \right. \\
&\quad \left. + zP_{gq}(z)\Sigma\left(\frac{x}{z},k^2\right) \right] \\
&- \left(1 - k^2\frac{\mathrm{d}}{\mathrm{d}k^2}\right)^2 \frac{k^2}{R^2} \int_x^1 \frac{\mathrm{d}z}{z} \\
&\quad \times \left[\int_{k^2}^{\infty} \frac{\mathrm{d}k'^2}{k'^4} \alpha_{\mathrm{s}}(k'^2) \ln\left(\frac{k'^2}{k^2}\right) f\left(z,k'^2\right) \right]^2 . \quad (17)
\end{aligned}
$$

The first seven lines in (17) describe the linear unified BFKL/DGLAP evolution [20]. Thus the second, third and fourth lines of this equation correspond to the BFKL evolution [7,26]. The constraint $\Theta\left(\frac{k^2}{z}-k'^2\right)$ reflects the so-called consistency constraint [27] which generates a dominant part of the subleading BFKL corrections [28,29]. The two terms in the fifth, sixth and seventh line in (17) correspond to the DGLAP effects generated by that part of the splitting function $P_{gg}(z)$ which is not singular in the limit $z \to 0$ and by the quarks respectively, with $\Sigma(x,k^2)$ corresponding to the singlet quark distributions

$$\Sigma(x,k^2) = \sum_{q=u,d,s}(q+\bar{q}) + c + \bar{c} = V(x,k^2) + S_{uds} + S_c, \quad (18)$$

where V, S_{uds} and S_c denote the valence, the light sea quark and the charmed quark distributions respectively. The inhomogeneous term $\tilde{f}^{(0)}(x,k^2)$ is defined in terms of the input (integrated) gluon distribution:

$$\tilde{f}^{(0)}(x,k^2) = \frac{\alpha_s(k^2)}{2\pi}\int_x^1 \mathrm{d}z P_{gg}(z)\frac{x}{z}g\left(\frac{x}{z},k_0^2\right). \quad (19)$$

The non-linear screening contribution is given by the last term in (17), where R denotes the radius within which the gluons are expected to be concentrated. The structure of this contribution follows from the Balitzki–Kovchegov equation [12,13] adapted to the unintegrated gluon distribution $f(x,k^2)$ [24] and the details concerning the structure of this term are briefly discussed in Appendix A. The sea quark distributions which describe the structure functions are calculated from the unintegrated gluon distributions using k_t factorization.

Unlike the case of the leading $\ln(1/x)$ approximation, (17) cannot be reduced to the evolution equation in $\ln(1/x)$ that makes its numerical analysis rather cumbersome. This complication comes from the fact that the subleading BFKL effects and the non-singular DGLAP contribution introduce a non-trivial z-dependence of the kernel. We have however observed that at small x the linear version of (17) can be very well approximated by an (effective) evolution equation in $\ln(1/x)$ with the boundary condition provided at some moderately small value of x (i.e. $x = x_0 \sim 0.01$). The latter is obtained from the solution of the linear version of (17) in the region $x > x_0$. To be precise we have observed that at small x we can make the following approximations.

(1) The consistency constraint $\Theta(k^2/z - k'^2)$ of the BFKL kernel responsible for the subleading BFKL effects is replaced by the following effective (z-independent) term:

$$\Theta(k^2/z - k'^2) \to \Theta(k^2 - k'^2) + \left(\frac{k^2}{k'^2}\right)^{\omega_{\mathrm{eff}}}\Theta(k'^2 - k^2). \quad (20)$$

This replacement is motivated by the structure of the consistency constraint in the moment space, i.e.

$$\omega\int_0^1 \frac{\mathrm{d}z}{z}z^\omega\Theta(k^2/z - k'^2) = \Theta(k^2 - k'^2) + \left(\frac{k^2}{k'^2}\right)^\omega\Theta(k'^2 - k^2). \quad (21)$$

(2) We make the following replacement:

$$\int_x^1 \frac{\mathrm{d}z}{z}[zP_{gg}(z) - 2N_c]f\left(\frac{x}{z},k'^2\right) \to \bar{P}_{gg}(\omega=0)f(x,k'^2), \quad (22)$$

where $\bar{P}_{gg}(\omega)$ is a moment function of $zP_{gg}(z) - 2N_c$, i.e.

$$\bar{P}_{gg}(\omega) = \int_0^1 \frac{\mathrm{d}z}{z}z^\omega[(zP_{gg}(z) - 2N_c]. \quad (23)$$

This approximation corresponds to keeping the leading term in the expansion of $\bar{P}_{gg}(\omega)$ around $\omega = 0$, which is a standard approximation at low x [30].

(3) We neglect the quark contribution in the right hand side of (17).

Using these approximations, (17) can be rearranged into the following form:

$$\frac{\partial f(x,k^2)}{\partial\ln(1/x)} = K_{\mathrm{L}}^{\mathrm{eff}}\otimes f - \int_{k_0^2}^\infty \mathrm{d}k''^2 K_S(k^2,k''^2)\left(1 - k''^2\frac{\mathrm{d}}{\mathrm{d}k''^2}\right)^2\left(\frac{k''^2}{R^2}\right), \times\left[\int_{k''^2}^\infty \frac{\mathrm{d}k'^2}{k'^4}\ln\left(\frac{k'^2}{k''^2}\right)\alpha_s(k'^2)f(x,k'^2)\right]^2, \quad (24)$$

where

$$K_{\mathrm{L}}^{\mathrm{eff}}\otimes f = 2N_c\frac{\alpha_s(k^2)}{2\pi}\int_{k_0^2}^\infty \mathrm{d}k''^2 \times\left\{\delta(k^2 - k''^2) + \Theta(k^2 - k''^2)\bar{P}_{gg}(0)\frac{\alpha_s(k''^2)}{2\pi} \times\exp\left[\bar{P}_{gg}(0)(\xi(k^2) - \xi(k''^2)\right]\right\} \times k''^2\int_{k_0^2}^\infty\frac{\mathrm{d}k'^2}{k'^2} \times\left\{\frac{f(x,k'^2)\left[\Theta(k''^2 - k'^2) + \left(\frac{k''^2}{k'^2}\right)^{\omega_{\mathrm{eff}}}\Theta(k'^2 - k''^2)\right] - f(x,k''^2)}{|k'^2 - k''^2|} + \frac{f(x,k''^2)}{[4k'^4 + k''^4]^{\frac{1}{2}}}\right\}, \quad (25)$$

$$K_S(k^2,k''^2) = \delta(k^2 - k''^2) + \Theta(k^2 - k''^2)\bar{P}_{gg}(0)\frac{\alpha_s(k''^2)}{2\pi} \times\exp\left[\bar{P}_{gg}(0)(\xi(k^2) - \xi(k''^2)\right]. \quad (26)$$

and

$$\xi(k^2) = \int_{k_0^2}^{k^2}\frac{\mathrm{d}k'^2}{k'^2}\frac{\alpha_s(k'^2)}{2\pi}. \quad (27)$$

Following [20] we set $k_0^2 = 1\,\mathrm{GeV}^2$. The method of the solution of (24) is described in Appendix B.

At first we solved the linear version of (24) with the non-linear term neglected starting from the initial conditions at $x = 10^{-2}$ obtained from the solution of the exact equation. The parameter ω_{eff} was then obtained by fitting the solution of the linear version of the approximate equation (24) to the solution of the linear version of the exact equation (17) of the unified BFKL/DGLAP framework. This procedure gives $\omega_{\mathrm{eff}} = 0.2$. It turns out that the solution of the linear version of the approximate equation (24) reproduces the solution of the linear version of (17) within 3% accuracy in the region $10^{-2} > x > 10^{-8}$ and $2\,\mathrm{GeV}^2 < k^2 < 10^6\,\mathrm{GeV}^2$).

We next solved the non-linear equation (24) setting $R = 4\,\mathrm{GeV}^{-1}$. The quark distributions defining the struc-

ture functions $F_{2,L}^{\mathrm{CC,NC}}$ were calculated from the k_t factorization [3,20]

$$2xq(x,Q^2) = \int \frac{\mathrm{d}k^2}{k^2} \int_x^{a_q(k^2)} \frac{\mathrm{d}z}{z} S_q^{\mathrm{box}}(z,k^2,Q^2) f\left(\frac{x}{z},k^2\right), \quad (28)$$

where the impact factors corresponding to the quark box contributions to the gluon–boson fusion process are the same as those used in [20] (see also [31]), i.e.,

$$S_q^{\mathrm{box}}(z,k^2,Q^2) = \frac{Q^2}{4\pi^2 k^2} \int_0^1 \mathrm{d}\beta \mathrm{d}^2\boldsymbol{\kappa'} \alpha_{\mathrm{s}} \delta(z-z_0) \times \left\{ [\beta^2+(1-\beta)^2] \left(\frac{\boldsymbol{\kappa}}{D_{1q}} - \frac{\boldsymbol{\kappa}-\mathbf{k}}{D_{2q}}\right)^2 + [m_q^2 + 4Q^2\beta^2(1-\beta)^2 \left(\frac{1}{D_{1q}} - \frac{1}{D_{2q}}\right)^2 \right\}, \quad (29)$$

where $\boldsymbol{\kappa'} = \boldsymbol{\kappa} - (1-\beta)\mathbf{k}$ and

$$D_{1q} = \kappa^2 + \beta(1-\beta)Q^2 + m_q^2,$$
$$D_{1q} = (\kappa - k)^2 + \beta(1-\beta)Q^2 + m_q^2,$$
$$z_0 = \left[1 + \frac{\kappa'^2 + m_q^2}{\beta(1-\beta)Q^2} + \frac{k^2}{Q^2}\right]^{-1}. \quad (30)$$

To be precise in the calculation of the (effective) quark distributions appearing in the charged current structure function we use the impact factors (29) corresponding to the massless quarks, and the (charmed) quark mass effects are included in the threshold factors:

$$a_{c,s}(k^2) = \left(1 + \frac{k^2+m_c^2}{Q^2}\right)^{-1}. \quad (31)$$

The k_t factorization formulas (28) and (29) contain subleading $\ln(1/x)$ effects coming from the exact kinematics of the gluon–boson fusion process [32]. Complete NLO corrections to the impact factors are discussed in [33]. In the impact factors corresponding to the neutral currents we use (29) with $m_u = m_d = m_s = 0$ and $m_c = 1.4\,\mathrm{GeV}$. We also include non-perturbative contributions according to the prescription defined in [20]. The valence quark distributions were taken from [22]. In Figs. 5 and 6 we show the results of our calculation for $\sigma_{\mathrm{CC}} \equiv \sigma_\nu^{\mathrm{CC}}(E)$ and $\sigma_{\mathrm{NC}} \equiv \sigma_\nu^{\mathrm{NC}}(E)$ with and without screening corrections included and confront them with our previous estimate based upon the GBW model.

We can see that at ultra-high energies the cross-sections calculated within the unified BFKL/DGLAP framework supplemented by screening effects are larger than those calculated from the simple GBW model. The resulting cross-sections are still appreciably smaller than the cross-sections calculated within the linear BFKL/DGLAP framework with the screening effects neglected.

A reduction of the magnitude of the neutrino cross-section is a consequence of the fact that the non-linear screening effects slow down the increase of the structure functions with decreasing x. In Fig. 7 we show the charged current structure function $F_2^{\mathrm{CC}}(x,Q^2)$ plotted as a function of x at $Q^2 = M_W^2$ with and without screening corrections included. We can see that the screening effects reduce the magnitude of $F_2^{\mathrm{CC}}(x,Q^2=M_W^2)$ at $x = 10^{-8}$ by almost a factor equal to two.

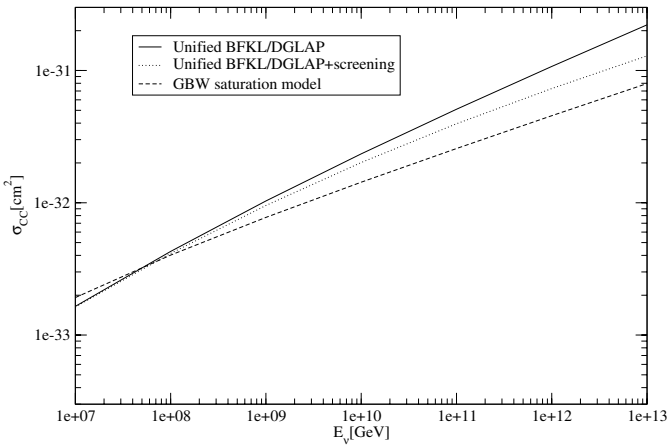

Fig. 5. The prediction for the neutrino–nucleon CC cross-section obtained from the unified BFKL/DGLAP equation supplemented by screening effects. For comparison we also present results based on the GBW saturation model and the linear unified BFKL/DGLAP evolutions

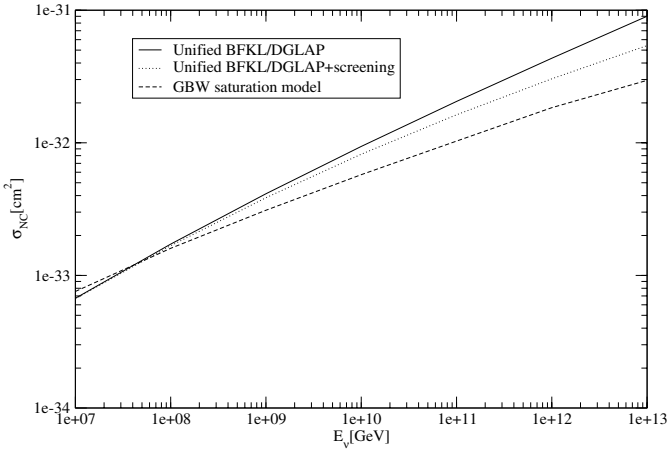

Fig. 6. As for Fig. 5, but for the NC interactions

The screening effects in structure functions are generated through k_t factorization by the screening effects in the unintegrated gluon distribution $f(x,k^2)$ which satisfies the non-linear equation (24). The non-linear screening corrections generate the critical line $Q_c^2(x)$ which increases with decreasing x which divides the k^2, x plane into two regions.

In the region $k^2 < Q_c^2(x)$ the unintegrated gluon distribution saturates, i.e. $f(k^2,x) \sim R^2k^2h(x,k^2)$, where $h(x,k^2)$ is a slowly varying function of x and k^2. In this region the unintegrated gluon distribution becomes much smaller than the solution $f_l(k^2,x)$ of the linear version of (24), which behaves approximately as $f_l(k^2,x) \sim x^{-\lambda}$

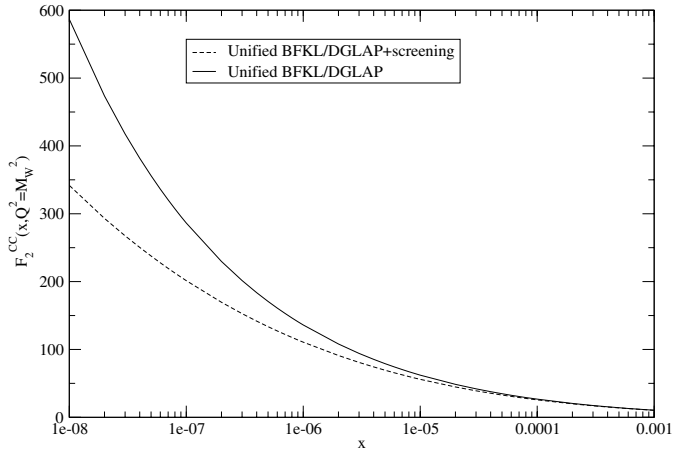

Fig. 7. The $F_2^{\rm CC}(x,Q^2)$structure function obtained from the unified BFKL/DGLAP equation supplemented by screening efects compared to results based on the linear BFKL/DGLAP evolution. The function $F_2^{\rm CC}(x,Q^2)$ is plotted as a function of x for $Q^2 = M_W^2$

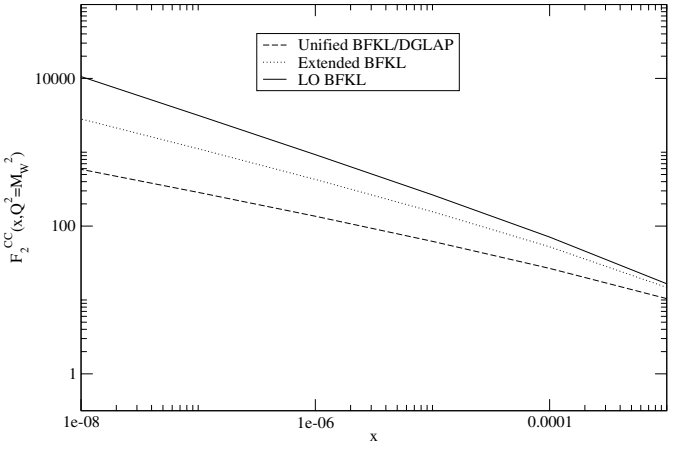

Fig. 8. The comparison of the $F_2^{\rm CC}$ structure function calculated for $Q^2 = M_W^2$ obtained from the unified BFKL/DGLAP evolution, extended BFKL evolution and LO BFKL evolution. Extended BFKL evolution corresponds to the BFKL equation with subleading effects generated by the consistency constraint but without the DGLAP effects

with $\lambda \sim 0.3$ over the entire region of k^2 [3,20]. In the region $k^2 > Q_c^2(x)$ the non-linear screening contribution on the right hand side of (24) becomes less important than the linear term and can be neglected for $k^2 >> Q_c^2(x)$. The magnitude of the unintegrated distribution continues to be significantly smaller than $f_l(x,k^2)$ over a substantial range of k^2. To be precise we have $f(k^2,x) \sim f(Q_c^2(x),x)$ with $f(Q_c^2(x),x) < f_l(k^2,x)$ in the region

$$\tilde{Q}^2(x) > k^2 > Q_c^2(x), \tag{32}$$

where $\tilde{Q}^2(x) = Q_c^4(x)/\Lambda^2_{\rm QCD}$ [34] [1]. It should be noted that $\tilde{Q}^2(x) >> Q_c^2(x)$. The screening effects do therefore significantly reduce the corresponding contribution to the k_t factorization integrals (28) coming from the region $k_0^2 < k^2 < \tilde{Q}^2(x)$. The integral over this region gives of course part of the leading twist contribution to the structure functions $F_2^{\rm CC,NC}(x,Q^2)$, which does not vanish at large Q^2. This result, that the screening effects for the structure function F_2 are appreciable even at such a large value, $Q^2 \sim M_W^2$, comes therefore from the fact that the screening effects contribute to the leading twist part of $F_2^{\rm CC,NC}(x,Q^2)$.

The fact that the screening effects at $F_2^{\rm CC,NC}(x,Q^2)$ can be important at $Q^2 \sim M_W^2$ and very small x ($x \sim 10^{-8}$) implies that they may in turn have a non-negligible influence on the ultra-high energy neutrino cross-sections. It is this fact which makes our results significantly different from those presented in [16,17] where the saturation effects were confined to the modification of the structure functions in the saturation region $Q^2 < Q_c^2(x)$ only. The corresponding contribution to the UHE neutrino cross-section coming from the integral over this region in (8) is very small and so modifications of the structure functions in the saturation region alone have a negligible impact on the UHE cross-sections [16,17].

The fact that the cross-sections are sensitive to the behavior at very small x and large scales $Q^2 \sim M_W^2$ implies that the effects which are formally subleading in $\ln(1/x)$ but can significantly affect both the $\ln(1/x)$ and the Q^2 evolution cannot be neglected. We illustrate this point in Fig. 8, where we show $F_2^{\rm CC}(x,Q^2)$ for $Q^2 = M_W^2$ calculated within three approximations: the leading $\ln(1/x)$ BFKL framework, the extended BFKL framework which includes the subleading $\ln(1/x)$ effects generated by the consistency constraint and the unified BFKL/DGLAP scheme which includes besides the BFKL dynamics with subleading effects also the complete DGLAP evolution.

The latter two frameworks contain effects which are subleading at low x. For simplicity of the presentation the non-linear screening effects are neglected in all three cases. We can see that both subleading $\ln(1/x)$ effects play a very important role and significantly reduce the magnitude of the structure function at large scale $Q^2 \sim M_W^2$ and very small values of $x \sim 10^{-8}$. Including these effects together with the screening contribution is therefore important for getting a reliable extrapolation of the structure functions into the region of very small values of x and large scales.

The discussion of the cross-sections performed so far concerned the screening effects on a nucleon target. In the case of neutrino–nucleus inelastic scattering a further reduction of the magnitude of the total neutrino cross-sections due to nuclear shadowing is expected [36]. In order to perform an indicative estimate of the possible nuclear shadowing effects for different values of the atomic numbers A we just modify the strength of the non-linear term in (17) by a factor $A^{1/3}$. In Fig. 9 we show our results for the normalized neutrino–nucleus cross-sections for differ-

[1] The condition (32) has a simple origin. It comes from the fact that possible scaling violations in the region $k^2 > Q_c^2(x)$ which modify the boundary condition provided along the critical line $Q_c^2(x)$ are approximately controlled by the "evolution length" $\tilde{\xi}(k^2,x) \sim \alpha_{\rm s}(Q_c^2(x))\ln(k^2/Q_c^2(x))$. The condition (32) is equivalent to the requirement $\tilde{\xi}(k^2,x) << 1$

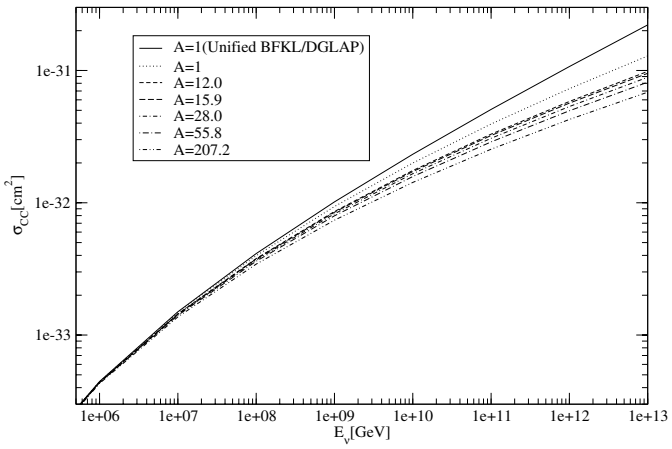

Fig. 9. The prediction for the neutrino–nucleus CC cross-section obtained from the unified BFKL/DGLAP equation supplemented by screening effects. The cross section is calculated for different atomic numbers and is normalized to the nucleon. For comparison we also present results for the neutrino–nucleon CC cross-section based on the (linear) unified BFKL/DGLAP evolution

ent values of the atomic number A varying from $A = 12$ to $A = 207$.

For comparison we show results for the neutrino–nucleon cross-section with and without screening effects. We see from this figure that nuclear shadowing can lead to a further reduction of the cross-section.

5 Summary and conclusions

In this paper we have performed an analysis of possible implications of the screening effects on the extrapolation of the neutrino–nucleon cross-sections towards the ultra-high energy region. The behavior of the cross-sections in this region probes the structure functions at very small values of x and relatively large scales $Q^2 \sim M^2_{W,Z}$. The values of x which can be probed can be as small as 10^{-8} and it may be expected that the parton densities in this ultra-small x region should be affected by non-linear screening effects which tame the indefinite increase of the parton distributions generated by a linear (BFKL and/or DGLAP) QCD evolution. At first we have performed an estimate of the total neutrino–nucleon cross-sections within the Golec-Biernat–Wüsthoff saturation model. In this model deep inelastic lepton scattering is viewed as the result of the interaction of the color $q\bar{q}$ dipoles which the gauge boson fluctuates to. An important ingredient of the model is the fact that it incorporates the saturation property of the total dipole–nucleon proton cross-section at large transverse separations between the constituents of the dipole. We have found that the neutrino total cross-sections obtained within this model are at ultra-high neutrino energies significantly smaller than those estimated from the linear BFKL/DGLAP evolution which neglects screening effects. We have observed however that part of this reduction might have been caused by the fact that the GBW model did not include the QCD evolution effects, and so it was not sufficiently accurate at very small values of x and large values of the scale $Q^2 \sim M^2_{W,Z}$. In order to overcome this potential deficiency of the GBW model we have performed an estimate of the cross-section within the more elaborate framework based on the unified BFKL/DGLAP scheme supplemented by the non-linear screening effects. Contrary to the simple GBW model this framework contained the complete BFKL and DGLAP evolution, including the subleading BFKL contributions. We have shown that all these effects are important in the region of very small values of x and large scales, which is relevant for the interactions of ultra-high energy neutrinos. The non-linear screening effects were still found to reduce appreciably the neutrino cross-sections at ultra-high energies; yet their effects turn out to be milder than in the case of the simple GBW model. We have also presented a very approximate estimate of the nuclear shadowing effects on further reduction of the cross-sections.

To summarize we have shown that the screening effects may play a non-negligible role in the extrapolation of the neutrino cross-sections towards ultra-high energies.

Acknowledgements. We thank Krzysztof Golec-Biernat, Alan Matin and Anna Staśto for useful discussions. This research was partially supported by the Polish State Committee for Scientific Research (KBN) grants no. 2P03B 05119, 5P03B 14420.

Appendix A

In this appendix we derive the non-linear shadowing term on the right hand side of (24) starting from the Balitzki–Kovchegov equation. The basic quantity within this framework is the number of the color dipoles $N(r, \mathbf{b}, x)$ in a nucleon, where r denotes the transverse size of the dipole and b is the impact parameter. The quantity $N(\mathbf{r}, \mathbf{b}, x)$ is closely related to the total cross-section $\sigma(r, x)$ describing the interaction of the $q\bar{q}$ color dipole of transverse size r with a nucleon,

$$\sigma(r, x) = 2 \int \mathrm{d}^2\mathbf{b} N(\mathbf{r}, \mathbf{b}, x). \tag{33}$$

The dipole cross-section is related to the unintegrated gluon distribution $f(x, k^2)$ [35]:

$$\sigma(r, x) = \frac{8\pi^2}{N_c} \int \frac{\mathrm{d}k}{k^3} [1 - J_0(kr)] \alpha_\mathrm{s} f(x, k^2). \tag{34}$$

For simplicity we regard α_s as a fixed parameter and will put its argument at the end. It is convenient to introduce the functions $\tilde{N}(\mathbf{l}, \mathbf{b}, x)$ and $\tilde{n}(l, x)$ defined as below:

$$\tilde{N}(\mathbf{l}, \mathbf{b}, x) = \int \frac{\mathrm{d}^2\mathbf{r}}{2\pi r^2} \exp[\mathrm{i}\mathbf{l}r] N(\mathbf{r}, \mathbf{b}, x), \tag{35}$$

$$\tilde{n}(l, x) = \int \mathrm{d}^2\mathbf{b} \tilde{N}(\mathbf{l}, \mathbf{b}, x). \tag{36}$$

From (33), (34), (35) and (36) we get

$$\tilde{n}(l,x) = \frac{\pi^2}{N_c}\int_{l^2}^{\infty}\frac{\mathrm{d}k^2}{k^4}\ln\left(\frac{k^2}{l^2}\right)\alpha_{\mathrm{s}}f(x,k^2), \tag{37}$$

where we have used the following relation:

$$\int_0^{\infty}\frac{\mathrm{d}r}{r}J_0(lr)[1-J_0(kr)] = \Theta(k^2-l^2)\ln\left(\frac{k}{l}\right). \tag{38}$$

Equation (37) implies the following local relation between $\tilde{n}(l,x)$ and $f(x,l^2)$:

$$\left(1-l^2\frac{\mathrm{d}}{\mathrm{d}l^2}\right)^2 l^2 n(l,x) = \frac{\alpha_{\mathrm{s}}\pi^2}{N_c}f(x,l^2). \tag{39}$$

In the large N_c limit the function $N(\mathbf{r},\mathbf{b},x)$ satisfies the Balitzki–Kovchegov equation [12,13]:

$$\begin{aligned} N(\mathbf{r}_{01},\mathbf{b},x) &= N_0(\mathbf{r}_{01},\mathbf{b},x) \\ &+ \frac{\alpha_{\mathrm{s}}N_c}{2\pi}\int_x^1\frac{\mathrm{d}z}{z}\left\{-2\ln\frac{r_{01}^2}{\rho^2}N(\mathbf{r}_{01},\mathbf{b},z)\right. \\ &\times\int_{\rho}^{\infty}\frac{\mathrm{d}^2\mathbf{r}_2}{\pi}\frac{r_{01}^2}{r_{02}^2r_{12}^2}\left[2N\left(\mathbf{r}_{02},\mathbf{b}+\frac{1}{2}\mathbf{r}_{12},z\right)\right. \\ &\left.\left.- N\left(\mathbf{r}_{02},\mathbf{b}+\frac{1}{2}\mathbf{r}_{12},z\right)N\left(\mathbf{r}_{12},\mathbf{b}-\frac{1}{2}\mathbf{r}_{20},z\right)\right]\right\}. \end{aligned} \tag{40}$$

The term linear in N on the right hand side of (40) corresponds to the right hand side of the BFKL equation (in transverse coordinate space) in the leading $\ln(1/x)$ approximation and the non-linear term describes screening effects. Taking the Fourier–Bessel transform of both sides of (40), integrating over $\mathrm{d}^2\mathbf{b}$ using the approximation $b >> 1/2r_{20}$ and $b >> 1/2r_{10}$ in the non-linear term and assuming the following factorization:

$$\tilde{N}^2(\mathbf{l},\mathbf{b},z) = \tilde{n}(l,x)S(b), \tag{41}$$

with

$$\int \mathrm{d}^2\mathbf{b}S(b) = 1, \tag{42}$$

we get

$$\begin{aligned} &l^2\tilde{n}(l,x) \\ &= l^2\tilde{n}^0(l^2,x) + \frac{N_c\alpha_{\mathrm{s}}}{\pi}\int_x^1\frac{\mathrm{d}z}{z}\left[K\otimes l^2\tilde{n} - \frac{1}{\pi R^2}l^2\tilde{n}^2(l,z)\right], \end{aligned} \tag{43}$$

where

$$\frac{1}{\pi R^2} = \int \mathrm{d}^2\mathbf{b}S^2(b). \tag{44}$$

The kernel K in (43) is the LO BFKL kernel. Using (37) and (39) we transform (43) into an equation for the unintegrated gluon distribution:

$$\begin{aligned} f(x,k^2) &= f^0(x,k^2) \\ &+ \int_x^1\frac{\mathrm{d}z}{z}\left\{\frac{N_c\alpha_{\mathrm{s}}}{\pi}K\otimes f - \left(1-k^2\frac{\mathrm{d}}{\mathrm{d}k^2}\right)^2\left(\frac{k^2}{R^2}\right)\right. \\ &\left.\times\left[\int_{k^2}^{\infty}\frac{\mathrm{d}k'^2}{k'^4}\alpha_{\mathrm{s}}(k'^2)\ln\left(\frac{k'^2}{k^2}\right)f(z,k'^2)\right]^2\right\}, \end{aligned} \tag{45}$$

where following [21] we set the argument of α_{s} equal to k'^2 in the non-linear term. Finally supplementing the linear evolution by the subleading BFKL effects generated by the consistency constraint and the DGLAP contributions resulting from the non-singular parts of the P_{gg} splitting function and quarks, we get (17). Following [20] we set the argument of α_{s} in the linear term equal to k^2.

Appendix B

In order to solve (24) we use the Tchebyshev interpolation formula:

$$f(x,k^2) = \frac{2}{N}\sum_{n,i=0}^{N-1}v_nT_n(\tau_i)T_n(\tau_{k^2})f(x,k_i^2), \tag{46}$$

where the $T_n(z)$ are the Tchebyshev polynomials, $v_0 = 1/2$ and $v_n = 1$ for $n > 0$. The variables τ_{k^2}, τ_i and k_i^2 are defined as

$$\tau_{k^2} = \frac{\ln\left(\frac{k^2}{k_{\max}k_0}\right)}{\ln\left(\frac{k_{\max}}{k_0}\right)}, \tag{47}$$

$$\tau_i = \cos\left(\frac{2i+1}{2N}\pi\right), \tag{48}$$

$$k_i^2 = k_{\max}k_0\left(\frac{k_{\max}}{k_0}\right)^{\tau_i}, \tag{49}$$

where we set $k_0^2 = 1\,\mathrm{GeV}^2$, $k_{\max}^2 = 10^6\,\mathrm{GeV}^2$. Combining the Tchebyshev interpolation formula (46) with (24) we reduce this equation to a system of the non-linear differential equations for the functions $f(x,k_i^2)$. This system is solved using the standard Runge–Kutta method and the function $f(x,k^2)$ calculated from (46) for arbitrary values of k^2 in the region $k_0^2 < k^2 < k_{\max}^2$. In the region $k^2 > k_{\max}^2$, which gives a negligible contribution anyway, we approximate the function $f(x,k^2)$ by $f(x,k_{\max}^2)$.

References

1. A. Kusenko, hep-ph/0203002; D. Hooper, hep-ph/0203239; F. Halzen, D. Hooper, Rept. Prog. Phys. **65**, 1025 (2000) and references therein
2. R. Ghandi, C. Quigg, M. Reno, I. Sarcevic, Astropart. Phys. **5**, 81 (1996); Phys. Rev. D **58**, 093009 (1998)
3. J. Kwieciński, A.D. Martin, A.M. Staśto, Phys. Rev. D **59**, 093002 (1999)
4. M.Glück, S. Kretzer, E. Reya, Astropart. Phys. **11**, 327 (1999)
5. R. Fiore et al., hep-ph/0302251
6. A.M. Cooper-Sarkar, R.C.E. Devenish, A. De Roeck, Int. J. Mod. Phys. A **13**, 3385 (1998)
7. L.V. Gribov, E.M. Levin, M.G. Ryskin, Phys. Rep. **100**, 1 (1983)
8. A.H. Mueller, J. Qiu, Nucl. Phys. B **268**, 427 (1986); A.H. Mueller, Nucl. Phys. B **415**, 373 (1994); B **437**, 107 (1995); A.H. Mueller, B. Patel, Nucl. Phys. B **425**, 471 (1994); Z.

Chen, A.H. Mueller, Nucl. Phys. B **451**, 579 (1995); A.H. Mueller, hep-ph/9911289; hep-ph/011244; A.H. Mueller, D.N. Triantafyllopoulos, Nucl. Phys. **640**, 331 (2002)
9. J. Bartels, G.A. Schuler, J. Blümlein, Z. Phys. C **50**, 91 (1991); Nucl. Phys. Proc. Suppl. C **18**, 147 (1991); J. Bartels, E.M. Levin, Nucl. Phys. B **558**, 617 (1992); J.C. Collins, J. Kwieciński, Nucl. Phys. B **335**, 89 (1990); E. Levin, K. Tuchin, Nucl. Phys. B **573**, 833 (2000); Nucl. Phys. A **691**, 779 (2001); Nucl. Phys. A **693**, 787 (2001); E. Gotsman, E. Levin, M. Lublinsky, U. Maor, hep-ph/0209074
10. L.D. McLerran, R. Venugopalan, Phys. Rev. D **49**, 2233, 3352 (1994); D **50**, 2225 (1994); A. Kovner, L. McLerran, H. Weigert, Phys. Rev. D **52**, 6231, 3809 (1995); J. Jalilian-Marian, A. Kovner, L. McLerran, H. Weigert, Phys. Rev. D **55**, 5414 (1997); J. Jalilian-Marian, A. Kovner, H. Weigert, Phys. Rev. D **59**, 014014, 014015, 034007, 099903, Erratum (1999); A. Kovner, J. Guilherme Milhano, H. Weigert, Phys. Rev. D **62**, 114005 (2000); R. Venugopalan, Acta. Phys. Polon. B **30**, 3731 (1999); E. Iancu, A. Leonidov, L.D. McLerran, Nucl. Phys. A **692**, 583 (2001); Phys. Lett. B **510**, 133 (2001); E. Ferreiro, E. Iancu, A. Leonidov, L.D. McLerran, Nucl. Phys. A **703**, 489 (2002); L.D. McLerran, Acta. Phys. Polon. B **33**, 2859 (2002); E. Iancu, K. Itakura, L.D. McLerran, hep-ph/0212123
11. K. Golec-Biernat, L. Motyka, A.M. Staśto, Phys. Rev. D **65**, 074037 (2002); K. Golec-Biernat, J. Phys. G **28**, 1057 (2002); Acta Phys. Polon. B **33**, 2771 (2002)
12. I. Balitzki, Nucl. Phys. B **463**, 99 (1996)
13. Yu.V. Kovchegov, Phys. Rev. D **60**, 034008 (1999); D **61**, 074018 (2000)
14. A.D. Martin, M.G. Ryskin, A.M. Staśto, hep-ph/0302140
15. D.A. Dicus, S. Kretzer, W.W. Repko, C. Schmidt, Phys. Lett. B **514**, 103 (2001)
16. M.H. Reno et al., hep-ph/0110235
17. R. Basu, D. Choudhury, S. Majhi, JHEP **0210**, 012 (2002)
18. J. Jalilian-Marian, hep-ph/0301238
19. K. Golec-Biernat, M. Wüsthoff, Phys. Rev. D **59**, 014017 (1999); D **60**, 114023 (1999)
20. J. Kwieciński, A.D. Martin, A.M. Staśto, Phys. Rev. D **56**, 3991 (1997); Acta Phys. Polon. B **28**, 2577 (1997)
21. J. Bartels, K. Golec-Biernat, H. Kowalski, Phys. Rev. D **66**, 014001 (2002); Acta Phys. Polon. B **33**, 2853 (2002)
22. M. Glück, E. Reya, A. Vogt, Z. Phys. C **67**, 433 (1995)
23. R.G. Roberts, The structure of the proton (Cambridge University Press, 1993)
24. M.A. Kimber, J. Kwieciński, A.D. Martin, Phys. Lett. B **508**, 58 (2001)
25. S. Catani, M. Ciafaloni, F. Hautmann, Phys. Lett. B **242**, 97 (1990); Nucl. Phys. B **366**, 657 (1991); S. Catani, F. Hautmann, Nucl. Phys. B **427**, 475 (1994); J.C. Collins, R.K. Ellis, Nucl. Phys. B **360**, 3 (1991)
26. E.A. Kuraev, L.N. Lipatov, V.S. Fadin, Zh. Eksp. Teor. Fiz. **72**, 373 (1977) [Sov. Phys. JETP **45**, 199 (1977)]; Ya.Ya. Balitzki, L.N. Lipatov, Yad. Fiz. **28**, 1597 (1978) [Sov. J. Nucl. Phys. B **28**, 822 (1978)]; J.B. Bronzan, L.R. Sugar, Phys. Rev. D **17**, 585 (1978); T. Jaroszewicz, Acta Phys. Polon. B **11**, 965 (1980)
27. M. Ciafaloni, Nucl. Phys. B **296**, 49 (1988); B. Andersson, G. Gustafson, J. Samuelsson, Nucl. Phys. B **467**, 443 (1996); B. Andersson, G. Gustafson, H. Kharraziha, J. Samuelsson, Z. Phys. C **71**, 613 (1996)
28. V.S. Fadin, M.I. Kotsky, R. Fiore, Phys. Lett. B **359**, 181 (1995); V.S. Fadin, M.I. Kotsky, L.N. Lipatov, hep-ph/9704267; V.S. Fadin, L.N. Lipatov, Phys. Lett. B **429**, 127 (1998); G. Camici, M. Ciafaloni, Phys. Lett. B **386**, 341 (1996); Phys. Lett. B **412**, 396 (1997) [Erratum B **417**, 390 (1997)]; Phys. Lett. B **430**, 349 (1998)
29. G.P. Salam, Acta Phys. Polon. B **30**, 3679 (1999)
30. J. Kwieciński, Z. Phys. C **29**, 561 (1985); R.K. Ellis, Z. Kunszt, E.M. Levin, Nucl. Phys. B **420**, 517 (1994) [Erratum B **433**, 498 (1995)]; R.K. Ellis, F. Hautmann, B.R. Webber, Phys. Lett. B **348**, 582 (1995)
31. J. Bartels, C. Ewerz, Phys. Lett. B **492**, 56 (2000)
32. A. Białas, H. Navelet, R. Peschanski, Nucl. Phys. B **603**, 218 (2001)
33. J. Bartels, D. Colferai, S. Gieseke, A. Kyrieleis, Phys. Rev. D **66**, 094017 (2002); J. Bartels, D. Colferai, S. Gieseke, C.F. Qiao, Phys. Rev. D **63**, 056014 (2001) [Erratum D **65**, 079902 (2002)]
34. J. Kwieciński, A.M. Staśto, Phys. Rev. D **66**, 014013 (2002); E. Iancu, K. Itakura, L. McLerran, hep-ph/0205198
35. A. Białas, H. Navelet, R. Peschanski, Nucl. Phys. B **593**, 438 (2001)
36. J.A. Castro Pena, G. Parente, E. Zas, Phys. Lett. B **507**, 231 (2001)